Proceedings of the ASME 2010 3rd Joint US-European Fluids Engineering Summer Meeting and 8th International Conference on Nanochannels, Microchannels, and Minichannels
FEDSM-ICNMM2010
August 1-5, 2010, Montreal, Canada

FEDSM-ICNMM2010-30961

Nonlinear Finite Element Approach to Simulate Wake-Induced Oscillation in Transmission Line Span

Dmitry Snegovskiy, Jean-Louis Lilien
University of Liège (Belgium)

Abstract— Wake-induced oscillations (WIO) in transmission line bundle conductors are simulated using finite-element nonlinear formulation. This allows obtaining the conductor oscillations in the line spans equipped either with spacers or with spacer dampers. Within this approach, the interaction of subconductors due to the wake is represented using Simpson's aeroelastic model. A special force element is created to introduce the aerodynamic loads due to the wake. The aeroelastic properties of the wake force field are tuned to meet the wake-induced instability properties as measured by Price.
Extension of the wake interaction sample onto the full line span is done taking into account the inertia-stiffness properties of the line fittings (spacer dampers). It is emphasized that in WIO the ability of spacer (spacer damper) to transfer the loads and motions plays essential role. Thus, the transfer matrix logic to simulate the spacer, established by Diana, Rawlins and other researchers, is now transferred into the finite element model of WIO. Some important structural specifics of transmission line fittings are thus highlighted by the performed simulations.
All these developments are introduced into the FE package SAMCEF Mecano. Results of a series of calculations are presented to illustrate the feasibility of the established model. Comparison of FEM simulations to the benchmarking field test data is presented.

***Index Terms*— Transmission lines, vibration, wake induced vibrations, simulations, benchmark.**

1 INTRODUCTION

In this work we consider the overhead power transmission lines (OHL). Their specifics are related to the presence of cables (conductors) whose length between supporting towers may extend to some hundreds of meters with diameter near a very few centimers, made of aluminium-alloy, sometimes steel reinforced. These conductors are working at every day stress near 15% to 25% of UTS (ultimate tensile stress). The OHL components are exposed to a combination of natural actions – wind, rain, ice / snow / frost deposits.
Compared to other structural parts, conductors have the highest flexibility and very low structural self-damping (of the order of 0.1 % of critical damping or lower (EPRI, 2009)).
Since early fifties the increased energy demand gave a rise to large construction of high-voltage and extra-high-voltage overhead lines equipped with bundled electrical conductors (like shown on fig.1). For such arrangements there was noticed a kind of wind-induced oscillations (Blevins, 1990) originated by a zone of disturbed and retarded air flow (wake), that the cables located upwind (windward) cast onto the downwind (leeward) ones (Fig. 1). The effect of this phenomenon called Wake-Induced Oscillations (WIO) (Cigada et al, 1995; Claren et al, 1971; Hardy et al, 1995) resulted in fatigue damages of conductors (Fig. 2), failures of insulator strings and cable suspension hardware and fatigue failures of spacers.

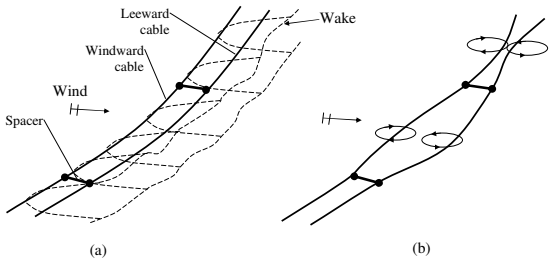

Figure 1. (a) Bundle conductors under wind: shielding of leeward conductor by the windward one caused by the wake. (b) Subspan oscillations – a typical case of wake-induced oscillations

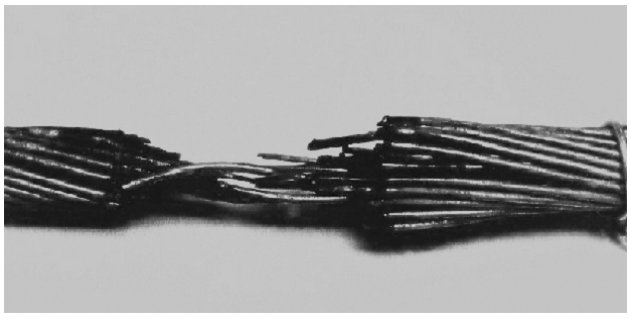

Figure 2. Severely damaged conductor under spacer clamp due to subspan oscillation [EPRI, 2009]

Manuscript received March 29, 2010. All authors are with University of Liège, department of electricity, electronics and computer sciences, Institut Montefiore, 4000 Liège, Belgium
J.L. Lilien is the corresponding author: +32-43662633; e-mail: lilien@ Montefiore.ulg.ac.be.
The authors kindly thank Samtech (www.samcef.com) who provides finite elment simulation tools using appropriate cable element to be completed by the detailed (in this paper) model giving access to the aeroelastic response of complex structures made of cables.

Other cable structures like suspenders in suspension bridges or stays in cable-stayed bridges are also subject to wake-induced oscillations (Simiu & Scanlan, 1996; Irvine, 1988). In each of these cases, conditions of oscillations' occurrence and structural response depend on cable's specific mass and stiffness, kind of fixation, dimension scale versus fluid viscosity and velocity (Reynolds number) etc. The cables' separation plays important role, as there are different kinds of wake interference especially when the cables are closely spaced.

A number of research projects were entertained to study the wake-induced oscillations of different structures, which brought to development of analytical and experimental models and methods of protection against this phenomenon (Diana et al, 1972; Laneville et al, 2001; Rawlins, 1976). A particular solution to overhead lines was found by unevenly distributing the spacers along the line span (Hearnshaw, 1974). To achieve that, no unique approach exists; virtually each grid company, or manufacturer of spacers proceeds with its own method. It may rely on different basis, either field experience or analytical study or a mixture of them.

2 NOTIONS OF WAKE

In the disturbed flow of the wind blowing onto the cable one distinguishes several zones (Fig. 3). The wake is the largest zone, consisting of succession of eddies, elongated downstream (Zdrakovitch, 1985 & 1987). There are different states of wake as function of the Reynolds number:

$$Re = \frac{VD}{\mu} \tag{2.1}$$

where D is cylinder's diameter, *m;* V the wind velocity, *m/s* , and μ the cinematic viscosity m^2/s (μ_{AIR} =1.5e-5 m^2/s).

The wake starts forming from $Re \approx 40$ as the *free shear layers* between accelerated flow (2) and retarded flow (1) start rolling up into alternating vortices. Their pattern known as Von Karman trail exists only at very low Re (up to 100…140). Further Re rises, the flow fluctuations disturb the wake stronger, making it turbulent. At $Re \approx 200$ turbulence involves the *far wake* , located at 40…50 cylinder diameters, and at $Re \approx 300\ldots400$ the *near-wake* becomes also turbulent.

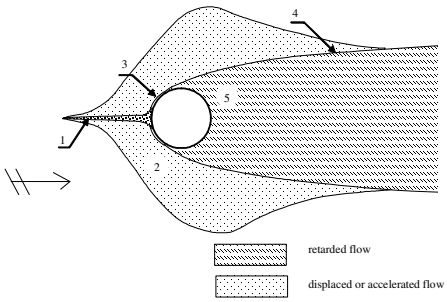

Figure 3. Regions of disturbed flow around cylinder (Zdravkovich):
(1) Narrow region of retarded flow;
(2) Displaced and accelerated flow;
(3) Boundary layer near the surface of cylinder;
(4) Free shear layer separating the accelerated flow and the wake;
(5) Wake

The state of the flow corresponding to low and normal wind velocities is denoted, after Zdravkovich, TrSL for "Transition in the Shear Layer". At this state, eddies result from rolling up of a shear-layer across the near-wake. When one growing eddy is strong enough to draw the other shear layer across the wake, the subsequent eddy is cut-off from a further supply of circulation. Hence the latter being shed from the cylinder at this stage, giving rise to a trail of alternate turbulent eddies. (Zdravkovich, 1987).

The above-described wake is characteristic to stranded electrical conductors at wind velocities U ~ 0.1 m/s to ~ 15 - 20 m/s.

Regarding the forces in the wake, we distinguish the high-frequency components of drag and lift, and quasi-stationary forces. The former ones are bound by the Strouhal number,

$$St = \frac{f_s D}{U}, \tag{2.2}$$

where f_s is the frequency of periodic vortex shedding from a structure (cylinder) of diameter D in a steady flow of velocity U . The latter ones are time-averaged and we pay to them most of attention, since for wake-induced oscillation of bundle conductors the quasi-steady hypothesis applies.

As mentioned above, further *Re* grows, the flow transitions to the turbulent state closer to the cylinder. Next to the free-shear layer, it is a boundary layer, circumscribing the surface of cylinder that is set to turbulent state. Simultaneously, the boundary layer becomes more 'sticky', so that the point of detachment into free shear layer moves behind along the surface of cylinder. The wake is getting narrower and the drag coefficient falling sharply. The resulting drag force stagnates in a region of drag coefficient fall; it is a phenomenon of drag crisis.

For the smooth cylinder this state, known as "transition into turbulence in boundary layer" (TrBL), occurs at *Re* ~2 x 10^5. Any surface roughness of cylinder reduces the critical level of *Re*. Conventional stranded conductors like ACSR Aster (diameter 30.5 mm) have transition state at U ~15 m/s and smooth conductors with their flattened surface of outer strands (like Compact or with Z-shaped strands) have critical *Re* value in-between the purely smooth cylinder and stranded conductors.

LOCAL VELOCITY IN THE WAKE

In the wake the mean velocity is retarded with respect to the free stream. This reduction in the far-wake can be approximately described by an empirical function 0. If we denote dimensionless horizontal and vertical spacing correspondingly $\xi = \frac{Y}{D}$, $\eta = \frac{Z}{D}$, and the free-stream drag coefficient C_{DMax} (for a smooth cylinder $C_{DMax} \cong 1.2$), then the ratio between the free-stream velocity, V , and the local velocity in the wake, $V_l(\xi,\eta)$ reads

$$b(\xi,\eta) = \frac{V_l(\xi,\eta)}{V} = 1. - C_{DMax} \cdot \sqrt{\frac{C_{DMax}}{(\xi + 6.0))}} \exp\left(-0.69 \cdot (\eta / B)^2\right);$$

where

$$B = 0.23\sqrt{C_{DMax} \cdot (\xi + 6.0)};$$

(2.3)

Selective profiles of the flow velocity retardation in the wake are shown in the Figure 4.

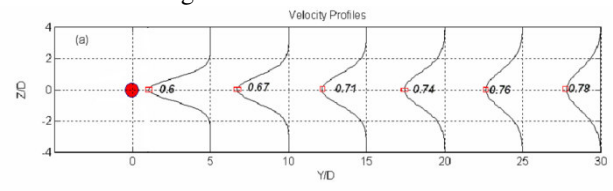

Figure 4. Selective profiles of velocity deficit $b(\xi,\eta)$ along the wake direction. Abscissa: horizontal dimensionless spacing (in cylinder diameters), ordinate: vertical dimensionless spacing.

LOADS ON THE LEEWARD CYLINDER IN THE WAKE

Now consider the downstream cylinder submerged in the wake of the same upstream cylinder. The time-averaged flow in the wake is directed towards the wake centreline. Effect of the flow retardation on the aerodynamics of the downstream cylinder may be compared to the one created by the airplane wing. The wing is specially profiled in order to form the retarded flow on its upper surface in order to create the lift force in the incident flow. In the wake, the flow distribution is such that the cylinder, originally neutral, is exposed to unevenly retarded flow. As result, the downstream cylinder obtains the reduced drag and nonzero lift, the latter being oriented towards the centreline of the wake.

A draft image of lift and drag distributions in the wake is presented in Figure 5. The drag (Fig 6) coefficient reflects the velocity retardation profile. The image of lift (Fig 6) coefficient corresponds to the derivative of drag coefficient by vertical coordinate, $C_{Dz}(y,z)$.

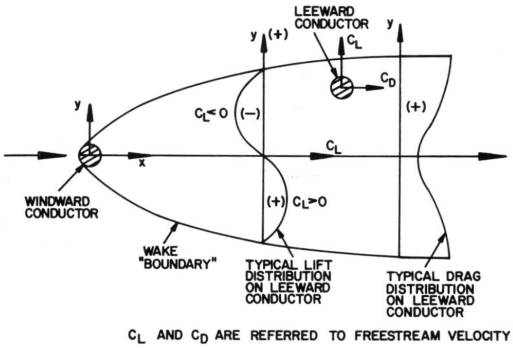

Figure 5. Aerodynamic forces on leeward conductor (EPRI, 2009)

Collection of aerodynamic coefficients on the leeward cylinders is presented by (Simpson, 1971), (Price, 1984), (Wardlaw et al., 1975), (Diana, 1972 &1999) and others contributed to the measures of loads imparted on smooth cylinders, smooth and stranded conductors in the wake.

Until nowadays wind-tunnel tests are the only credible source of information about wake-induced loads. An attempt of numerically obtaining the wake-induced lift and drag coefficients has been done by the authors using a CFD tool *FlowVision* (*www.flowvision.ru*) at Re 20k. Analysis has demonstrated, that such computation, in the best case, allows for obtaining the results more or less approaching to the experimental data.

An exemplary distribution of lift and drag coefficients, obtained by (Price,1975 & 1984) for a smooth cylinder is given in Figure 6. Notice that, as the separation between cylinders rises, the enlargement of the wake transmits into profiles of the aerodynamic coefficients.

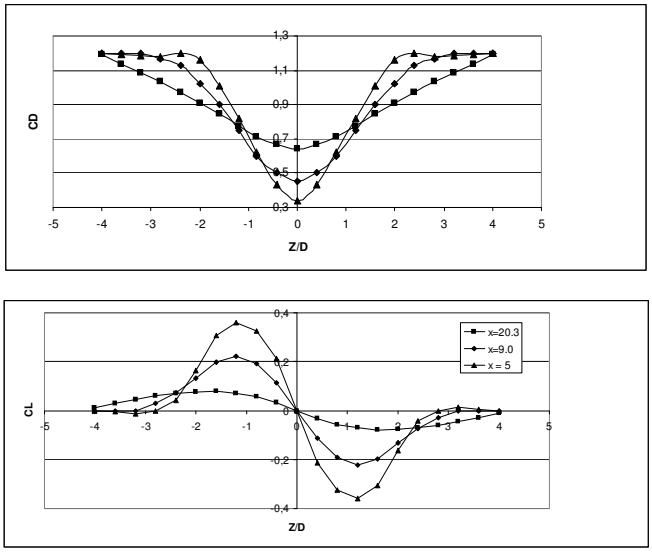

Figure 6. Force coefficients for a smooth circular cylinder with a free stream
Re = 3.58 x 10^4 and turbulence intensity 1.5 %. Markers denote cylinders' spacing, y/d: ○ – 5.0, ● – 9.0, Δ – 20.3. Data after [Price, 1975]

The wake narrowing in critical state (drag crisis) is obviously transferred into the loads on the leeward cylinder. Since, during oscillations the subconductors may approach up to clashing, consider the near-wake (within $0 \le |Y/D| < 5$). At such distance, the time-averaged coefficients acting on the leeward cylinder vary strongly across-wake. At distances less than Y/D = 3 the drag coefficient takes negative values.

As the leeward cylinder is at distance less than 1.5D, the windward cylinder's lift and drag coefficients are also affected (Price, 1984).

OVERVIEW OF WAKE-INDUCED OSCILLATION

The four principal types of wake-induced motion are illustrated in Fig. 7. Three of these types, B, C and D, are termed "rigid-body modes" since little distortion of the bundle cross-section occurs. They are similar to the fluttering motions of the ribbon. In each of these modes generally one of three degrees of freedom (vertical, horizontal or rotational) is dominant, however, other two are present.

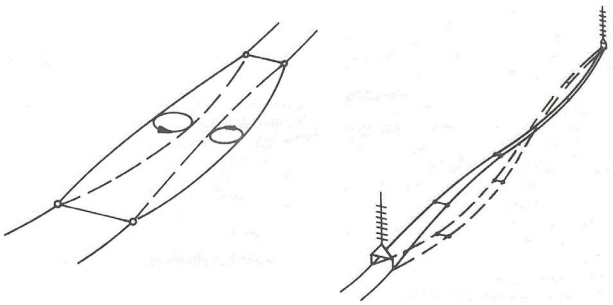

A. Subspan mode B. Vertical galloping

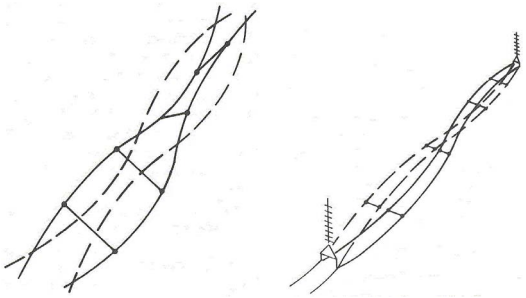

C. Horizontal mode or twisting D. Rolling or snaking

Figure 7. Classification of wake-induced motions [EPRI, 2009]

The subspan mode (Fig 7, A) takes the form of one or several loops between spacers in a span, with nodes at or near the spacers. The trajectories of individual subconductors are elliptical, and windward-leeward pairs of subconductors often move approximately in phase opposition. Motions in adjacent subspan are usually synchronized but are not necessarily in phase or exactly out-of phase. The one-loop-per-subspan form is the most common. More than two loops per subspan are rarely observed, except when the conductors are wet.

Detailed analysis of wake-induced oscillations over a whole span reveals that several modes participate in the motion at the same time (EPRI, 2009).

CONDITIONS OF OCCURRENCE

A number of conditions must be satisfied simultaneously in order the wake-induced oscillations may appear. The tilt of bundle with respect to the wind must be right, the subconductor separation expressed as a/d, the ratio of spacing a to the diameter d must not be too large, the spacing system and support arrangements must be amenable, and the wind must be of sufficient smoothness. The latter appears to be particularly restrictive. The ratio between in-plane/out-of-plane eigenfrequencies is also a key parameter (fig.8), it depends on the %UTS (ultimate tensile strength) used in the conductors.(Simpson, 1967)

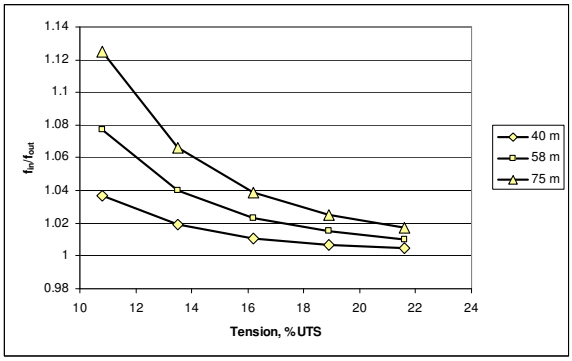

Figure 8. Influence of subspan length on relationship between in-plane/out-of-plane eigenfrequencies

In horizontal arrangement of the bundle, the leeward conductor is found in tandem behind the windward conductor, and is not susceptible to the wake-induced oscillation. The situation changes when the bundle is tilted due to different factors. One distinguishes positive and negative tilt, depending on location of leeward conductor in the upper or lower half of the wake correspondingly. Most observations of wake-induced oscillations in twin bundles corresponded to the positive tilt. In triple bundles the wake-induced oscillations are mostly observed at negative tilts.

There is no explanation found to justify why such difference occurs in twin and quad bundles' behaviour. In wind-tunnel tests for suspended twin cylinders at properties, similar to conductor bundles, the oscillations were observed at negative tilts, which have been supported by Simpson's theory (Simpson, 1971 & 1977) and his successors (Price, 1975 & 1990), (Tsui, 1976 & 1977 & 1986). A linear model which predicts twin bundle instability at positive tilt has been developed by (Rawlins, 1976).

This work is mainly based upon Simpson's theory, however, it also presents analysis results where twin bundle oscillates at positive tilt.

3 WAKE-INDUCED FLUTTER MODEL

Before going to finite element model, simple approach may be of interest. In this model the conductors' twin bundle is reduced to a rigidly fixed windward and elastically suspended leeward one (Fig 9). Such reduction is possible basically for two cases: that of telegraph wire, and of nearly equal subspans. The motion of leeward cylinder only is considered, as this is the motion that inhibits the subspan oscillation. The action of windward cylinder is considered only via space-dependent local velocity and lift and drag coefficients. Other authors have already treated similar approaches (Hartlen et al, 1970; Kern, 1995).

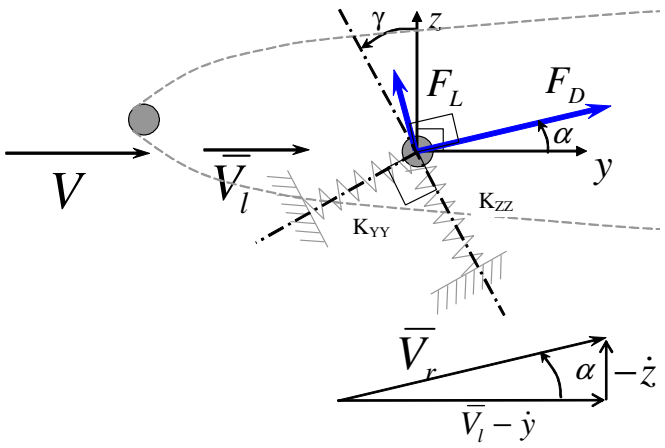

Figure 9. Wake-induced action on elastically suspended leeward cylinder

The state of leeward cylinder is described by a system of two equations of motion along two axes y and z:

$$\begin{cases} m\ddot{y} + 2m\zeta_Y \omega_Y \dot{y} + k_{YY} y + k_{YZ} z = F_Y \\ m\ddot{z} + 2m\zeta_Z \omega_Z \dot{z} + k_{ZZ} z + k_{YZ} y = F_Z \end{cases} \quad (3.1)$$

Here,

m [kg/m] mass per unit length of cylinder,

ζ_Y, ζ_Z critical damping ratio,

F_Y and F_Z [N/m] force components which result from the drag and lift forces acting on the leeward cylinder.

k_{YY}, k_{ZZ} and k_{YZ} [N/m] axial and coupled stiffnesses per unit length, N/m, resulting from inclination of the suspension and modelling the blowback of the bundle under the wind.

Forces F_Y and F_Z are axial components of the drag and lift forces which read

$$\begin{cases} F_L = \frac{1}{2}\rho V_r^2 \, d \, \tilde{C}_L \\ F_D = \frac{1}{2}\rho V_r^2 \, d \, \tilde{C}_D \end{cases} \quad (3.2)$$

Here, $\tilde{C}_D$ and $\tilde{C}_L$ are aerodynamic coefficients defined with respect to the local velocity, V_l; $\bar{V}_r$ is a vector resulting from subtraction of the local wind velocity and the speed of the leeward cylinder (see Figure9).

$$\bar{V}_r = \left(\bar{V}_l - \dot{\bar{y}}\right) + \left(-\dot{\bar{z}}\right) \quad (3.3)$$

Axial components of forces, F_Y and F_Z, relate to the drag and lift forces via relationships

$$\begin{cases} F_Y = F_D \cos\alpha - F_L \sin\alpha \\ F_Z = F_D \sin\alpha + F_L \cos\alpha \end{cases} \quad (3.4)$$

$\bar{V}_r$ is inclined to the axis y with an induced angle of attack, α

$$\begin{aligned} \cos\alpha &= \frac{V_l - \dot{y}}{V_r} \\ \sin\alpha &= \frac{-\dot{z}}{V_r} \end{aligned} \quad (3.5)$$

The aerodynamic coefficients, obtained experimentally, refer to the free-stream velocity, V. To make use of them, introduce the relationship between the « local » and «free-stream » coefficients as

$$\begin{Bmatrix} C_D \\ C_L \end{Bmatrix} = b^2 \cdot \begin{Bmatrix} \tilde{C}_D \\ \tilde{C}_L \end{Bmatrix}, \quad b^2 = \left(\frac{V_l}{V}\right)^2 \quad (3.6)$$

The coefficient b is found from the relationship (2.3).

By substitution of (3.2) - (3.6) into (3.1), we obtain the full equations of leeward cylinder motion,

$$\begin{cases} m\ddot{y} + 2m\zeta_Y \omega_Y \dot{y} + k_{YY} y + k_{YZ} z = qV_r \frac{1}{b^2}\left(C_D\left(V_l - \dot{y}\right) + C_L \dot{z}\right) \\ m\ddot{z} + 2m\zeta_Z \omega_Z \dot{z} + k_{YZ} y + k_{ZZ} z = qV_r \frac{1}{b^2}\left(-C_D \dot{z} + C_L\left(V_l - \dot{y}\right)\right) \end{cases} \quad (3.7)$$

Here, $q = \frac{1}{2}\rho d$ is the air pressure with ρ air density (1.22 kg/m^3), and d cylinder's diameter.

By solving this system numerically in time domain we can calculate the motion of leeward cylinder in order to obtain the limit cycle. However, this system does not tell anything about stability of leeward cylinder at the given wake location. To analyse this we suppose that leeward cylinder has been driven at the equilibrium position in the wake and consider the small motions around this position. So we linearize the equations of motion by passing from nonlinear lift and drag coefficients to their linear analogs by expanding them in Taylor series (not detailed here).

Next we regroup the terms at $\tilde{y}$, $\tilde{z}$ and their derivatives and obtain the system

$$M_{STR}\ddot{r} + \left[C_{AER} + C_{STR}\right]\dot{r} + \left[K_{AER} + K_{STR}\right] r = F_{AER} \quad (3.8)$$

Here,

$r = \begin{bmatrix} \tilde{y} \\ \tilde{z} \end{bmatrix}$ - column vector of displacement components;

$M_{STR} = \begin{bmatrix} m & 0 \\ 0 & m \end{bmatrix}$ - structural mass matrix;

$K_{STR} = \begin{bmatrix} k_{yy} & k_{yz} \\ k_{yz} & k_{zz} \end{bmatrix}$ - structural stiffness matrix (remind that suspension stiffnesses, K_{YY} and K_{ZZ} are expressed in terms of axial and coupled components, k_{yy}, k_{zz} and k_{yz});

$C_{AER} = q\frac{d}{V_l}\begin{bmatrix} 2C_D & -C_L \\ 2C_L & C_D \end{bmatrix}$ - aerodynamic damping matrix ($q = \frac{\rho V^2}{2}$);

$C_{STR} = 2\begin{bmatrix} \zeta & 0 \\ 0 & \zeta \end{bmatrix}$ structural damping matrix;

$K_{AER} = -q\begin{bmatrix} \tilde{C}_{D_Y} & \tilde{C}_{D_Z} \\ \tilde{C}_{L_Y} & \tilde{C}_{L_Z} \end{bmatrix}$ - aerodynamic stiffness matrix;

$F_{AER} = q\begin{bmatrix} C_D \\ C_L \end{bmatrix}$ column vector of aerodynamic forces at the equilibrium position.

We then study this system by bringing it to homogeneous form and investigating the stability of its complex eigenvalues.

AERODYNAMIC DATA

In wake-induced oscillations studies it is very important to rely upon good aerodynamic data. Among the data available for smooth cylinder two sources provide coefficients in the large range of spacings: that published by (Diana, 1972) and by (Price, 1984). For stranded conductor, the EPRI "Orange Book" (EPRI, 2009) provides a semi-empirical fit for Chukar conductor, distinctive by that it is dependent not only on space, but also on Reynolds number.

In our work we used the smooth cylinder data, keeping in mind that the conductor data can be used instead. Use of analytical expressions for C_D and C_L greatly simplifies the way to obtain the derivatives and, in finite-element analysis, it has accelerated the computation (Fig 10 & 11). It was of interest to apply aerodynamic data, obtained by Price. Advantage of these data is that they snapshot the enlargement of wake along the longitudinal spacing. Furthermore, in certain regions of wake their derivatives meet the condition of dynamic instability established by Simpson,

$C_{Ly}C_{Dz} < 0$

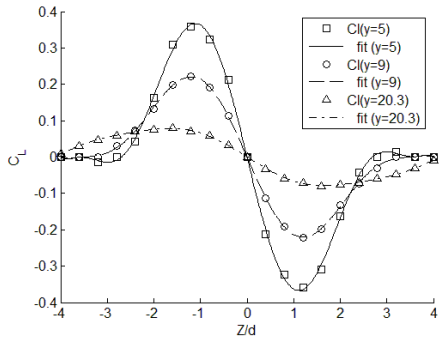

Figure10. Example of lift coefficient by z coordinate

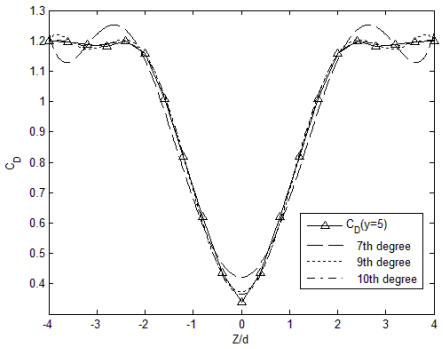

Figure11. Example of the drag coefficient with different polynomials

COMPARISON TO PREVIOUS STUDIES

First consider a case referred by (Price, 1975).

Cylinder suspension has following parameters:

Mass per unit length: $m = 2.5$ kg/m

Suspension out-of-plane frequency, $f_Y = 4.196$ Hz; in-plane frequency, $f_Z = 4.029$ Hz

Cylinders' diameter $d = 29.4$ mm

Incident flow velocity: $V = 20$ m/s (Re 39.2k)

Suspension inclination: $\psi = 15.5^\circ$ ($g = \tan\psi = 0.2678$)

Structural damping ratio: $\zeta = 0$.

Results are shown in Fig 12 (using also outputs from Price, 1975).

T2 contours are close to the Price's solution, and T3 and maximum real part of roots are more elongated.

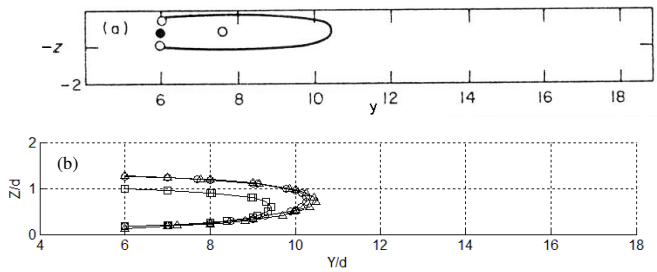

Figure 12. Flutter boundaries for a smooth circular cylinder, $V = 20$ m/s, Re 39.2k

(a) Price results, ○ – experimental, ___-theoretical.

(b) Present results – polynomial fit of aerodynamic data and analytical derivatives. Contours obtained by:- - : second Routh test function, T2; -○-: third Routh test function, T3; -Δ-: maximum real part of polynomial roots.

CRITICAL FLUTTER VELOCITY

Let us find the critical flutter velocities for a leeward cylinder. The incipience of critical velocity is well seen on the plot of solution real part versus incident flow velocity Figure13 & 14. Two real parts, $\varepsilon_1, \varepsilon_2$ corresponding to four complex conjugate eigenvalues, $\lambda_{1...4} = \varepsilon_{1,2} \pm i\omega_{1,2}$, when solved for increasing incident velocity, provide two branches. If unstable solution exists, one of branches rises to positive values.

This branch initially corresponds to the higher eigenfrequency of in-plane mode. As the solution approaches to instability, the eigenfrequencies become closer in order to coincide. Upon further growth of velocity, the eigenfrequencies remain close to each other, however, they cross-over. This image is similar to the flutter of aircraft wing.

It is interesting that in the system with inverse relationship of in-plane and out-of-plane frequencies, the in-plane mode is still the one which brings instability. Such case is shown in Figure15. In this case, where leeward cylinder is located in the upper half-wake, the eigenfrequencies approach, however, they do not fully synchronize. This probably indicates, that although the system is unstable, no steady oscillation would occur.

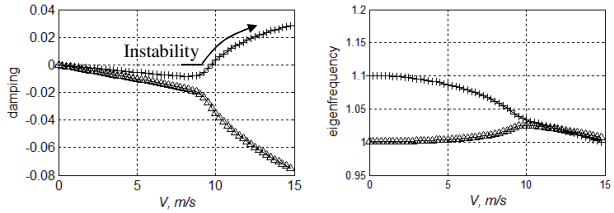

Figure 13. Onset of flutter velocity. cylinder diameter: 30 mm, mass 1.6 kg/m, horizontal spacing y/d = 10, vertical spacing z/d = -2.5, blowback angle $\psi = 15.5^\circ$. In-plane mode and out-of-plane mode.

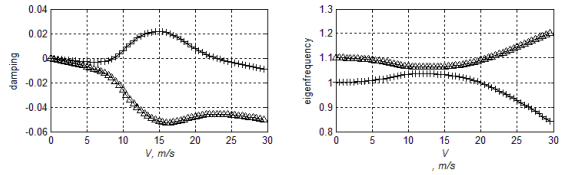

Figure 14. Onset of flutter velocity. cylinder diameter: 30 mm, mass 1.6 kg/m, horizontal spacing y/d = 14, vertical spacing z/d = 1.5, blowback angle $\psi = 15.5^\circ$. In-plane mode and out-of-plane mode.

Now consider the influence of structural damping ζ on the flutter boundaries and critical velocity. The normal self-damping in the conductors is about 0.1% of critical damping. Up to these values the flutter boundary is virtually insensitive to the damping at all. Only the augmentation by an order of value, to 1%, brings some shift to the greater frequency ratios. A considerable effect is possible with the damping 5%, but this level is not practically achievable. Interested readers may also have a look at (Mohajery & Rawlins, 1977; Rawlins, 1977)

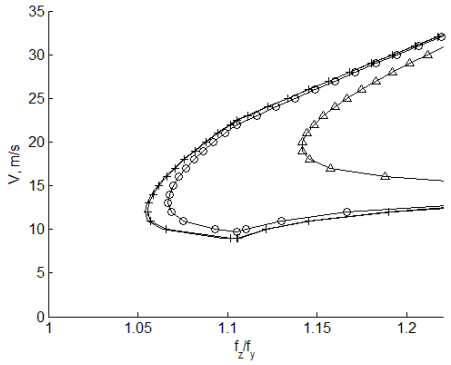

Figure15. Variation of critical velocity with frequency ratio: y/d = 16.32, z/d = -2.5; $f_y = 0.9 \to 1$; $f_z = 1.1 \to 1$; cylinder mass: 1.313 kg/m, diameter 24.5 mm, blowback 10°. ___ no damping; -+- damping 0.1%,;-o- damping 1%; -Δ- damping 5%

4 SAMCEF MECANO MODEL OF WAKE INTERACTION

The model described below summarizes the approach described in former Section to model the wake-induced interaction in twin conductor bundle. All implementations are done in the FE simulation package SAMCEF v12 (Samcef, 2009). Very few similar investigations have been done in the literature (Newman & Karniadakis, 1997; Tsui, 1986).

The model is based on user-defined element type MC531 which allows application of external forces to the nodes of cable. The forces are space- and time-dependent and are calculated on basis of lift and drag coefficients' distribution in the wake.

The routine *Simpson.f* obtains, at each time instance, the data on wind velocity and nodal locations for windward and leeward conductor. Based on these data it calculates the dimensionless components of spacing between cable nodes and transfers these data to *Waker3.f* for calculation of local velocity and, depending on location of leeward node in the wake, to the block of wake aerodynamic coefficients routines.

The aerodynamic data are stored in tabular form. To obtain a value in any location of cable node at any time instance, two approaches can be used:

- spline interpolation
- polynomial surface fit

The second approach is preferable for using wherever possible as it allows for saving the computation time.

NUMERICAL EXAMPLES

Single span 80 m long: twin bundle

A single span model of 80 m has been simulated to see the impact of the conditions to the subspan oscillations. Conductor spacing and initial tension are also close to a real span.

Input data

Parameters of model:

Span length:	Conductor diameter	Conductors horizontal spacing	Conductors vertical spacing
80 m	3 cm	16 conductor diameters	-2.5 conductor diameters (leeward conductor lower)

Conductor tension	Conductor mass per unitlength	In-plane frequency	Out-of-plane frequency	Frequency relationship
30000 N	1.25 kg/m	1.01 Hz	0.96 Hz	1.052

Parameters of aerodynamic loading

Wind velocity	Aerodynamic data
15 m/s	Price

Results

Calculation results are illustrated in Figure16. The elliptical orbit of leeward conductor in the middle of span has approx. 16.7 conductor diameters in the major axis and 3.3 conductor diameters in the minor axis. Note that the sag (of the sub-span) is about 0.3 m.

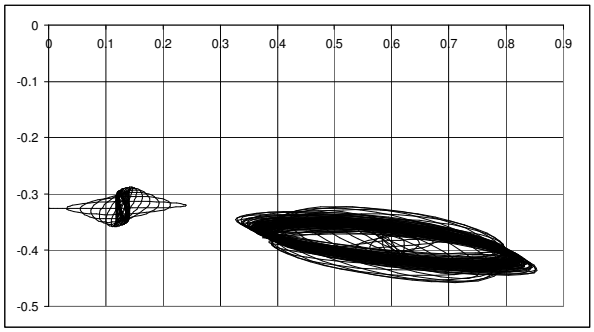

Figure16. WIO in the 45 m long single twin span. Left orbit: windward conductor, right orbit: leeward conductor

Note, that windward conductor makes typical free-decaying oscillations after being excited by initial wind impact (in this and other case studies, the wind grows from zero to the constant within the period of around 1 second).

BENCHMARK CASE

The benchmark test case was relevant to tests conducted at the Magdalen Island by IREQ and distributed during CIGRE WG activities (courtesy A. Manenti).

Quadruple bundle (450 mm separation) equipped with ACAR 1300 conductors (stranding 37 x 4.76). Tensile load 20% RTS (29.1 kN).
Span: 367 m. (between tower 2 and 3); 7 subspans: 35 - 56 - 64 - 57 - 65 - 55 - 35.
Bundle height:
Tower N°2: 24.85m; Tower N°3: 26.10m
Measurements (wind and oscillation amplitude in the various subspans): table 1

Theline was equipped with spacer-damper :
Torsional stiffness of the hinge: 294.3 Nm/rad,
Axial stiffness of the hinge: 820000 N/m,
Ratio between torsional damping and torsional stiffness: .32
Ratio between axial damping and axial stiffness: .32

Arm mass: 0 .7 kg
Arm mass moment of inertia with respect to the centre of mass: 1.67E-3 kg m^2
Central body mass: 2.25 kg
Central body mass moment of inertia with respect to the centre of mass: 65.72E-3 kg m^2
The spacer, whose dynamic properties are essential, as stated by (Hardy et al, 1980) has been modelled as follows (fig 17). A sine sweep excitation was applied to get the outputs as shown on fig 18.

Table 1 : observed peak-to-peak amplitudes.

Subspan	Subspan Length	Wind conditions			Yp-p
		velocity	direction	velocity normal comp	
no.	m	m/s	degree	m/s	mm
1	35	12.2	250	11.4	57.7
		11.4	249	10.7	51.3
2	56	18.2	244	16.3	117.5
		9.9	247	9.1	111
3	64	19.4	243	17.3	145.9
		10.1	246	9.2	64.6
4	57	18.7	243	16.7	95.1
		8.4	107	8.0	51
5	65	19.4	241	17.0	294.1
		11.2	246	10.2	80.6
6	55	19.4	241	17.0	273.5
		10.9	105	10.5	34.8
7	35	19.4	243	17.3	37.9
		11.9	293	11.0	25.6

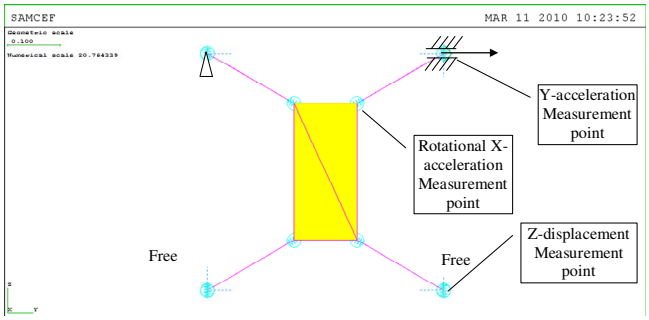

Fig 17 : finite element model of the spacer damper used in the benchmark case.

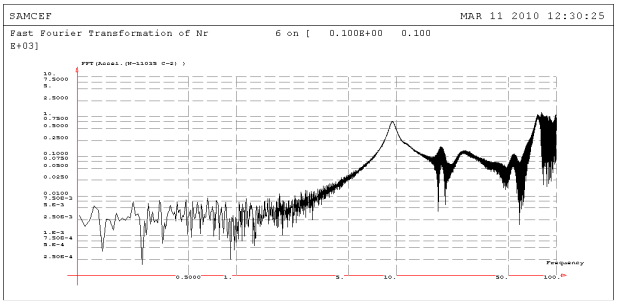

Fig 18: frequency response of the spacer damper.

It was clear that the spacer resonance frequencies were chosen against Aeolian vibration spectrum. The complex modal analysis of the spacer integrated into the bundled conductor also shows, that even if the spacer deformations contribute into the coupling of subspan modes, only starting of the frequency around 3 Hz its damping capacity becomes effective, still remaining quite low until aeolian vibration level (here around 8 Hz - see Fig.19). Thus, damping will be of no help on basic WIO range (typically here 1 Hz)

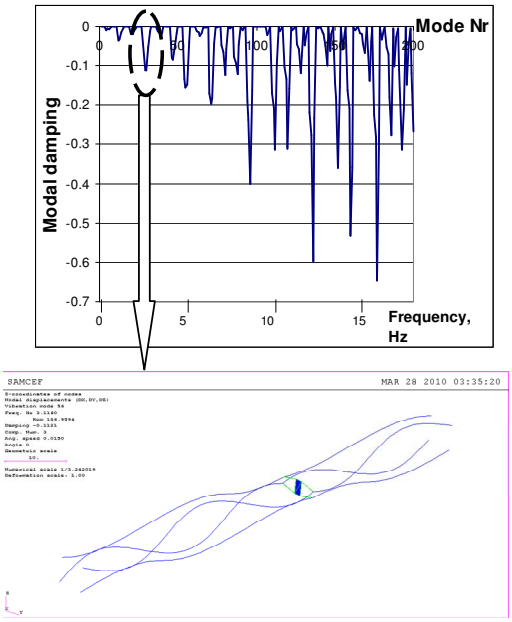

Fig 19: Modal damping of the spacer damper + two subspan bundle vs. eigenfrequency (above) and corresponding mode shape of the first noticeably damped mode (below).

The Fig. 20 is showing the full span modeled by finite element into SAMCEF code. The picture has been taken at a time when WIO occurred mainly on subspan 5.

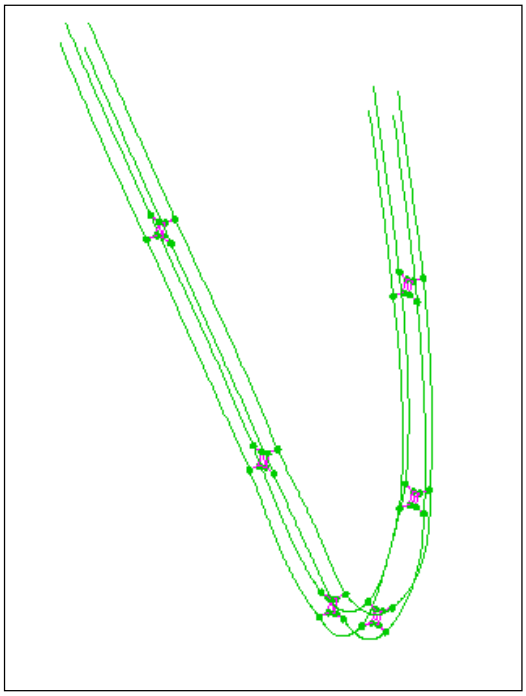

Fig 20: an instantaneous view of the full quad bundle modeled during WIO oscillations.

The following figures showed time response of the amplitude of the vibration. Fig. 21 starting from zero (application of the wind) and fig 22 with a zoom during WIO. Fig 23 is showing the same as fig 22 but in spacer plane.

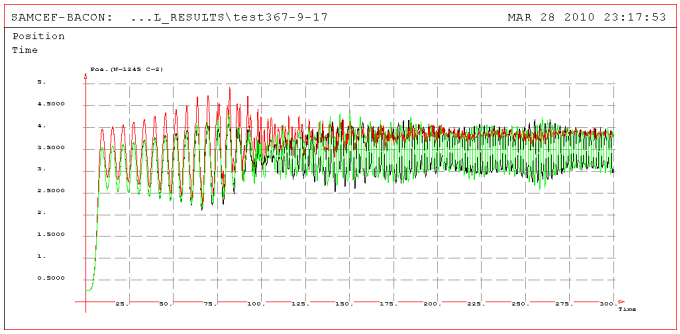

Fig 21: benchmark case. WIO on subspans 3-4-5 from early beginning of wind application.

The phenomenon of WIO has been reproduced by FE simulation. It was clear that , moreover to many other factors already detailed (tilt angle, in-span versus out-of-span frequency ratio, wind speed and direction), that the spacer had a dramatic influence on the phenomenon. That influence is manyfold : transmission of movement between subconductors, flexural and rotational stiffness.

Based on the fact that the range of frequency concerned by WIO (based on typical subspan length near 50 to 70 m, with conductor UTS near 20%), there are few hopes to be able to introduce damping to limit the phenomenon. Only appropriate

optimization procedure about the location of spacers, together with spacer data may lead to appropriate response to limit WIO.

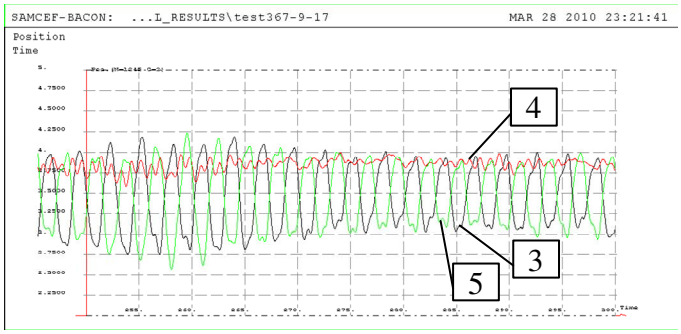

Fig 22 : benchmarck case. WIO on subspans 3-4-5 (zoom during WIO) showing a typical snaking mode (case D on Fig 7)

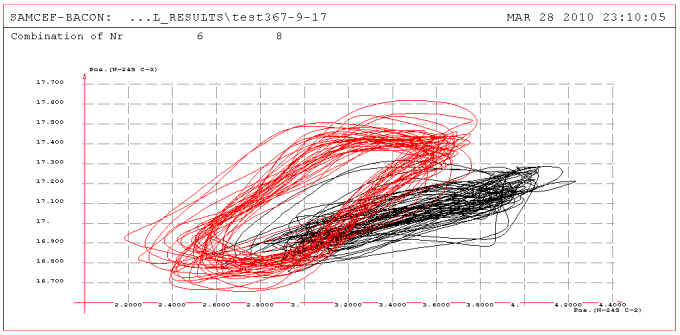

Fig 23 : Subspan 5 - movement of two subconductors of the bundle (upper ones), clearly showing that WIO has created a coupling (owing to the spacer) between both subconductors.

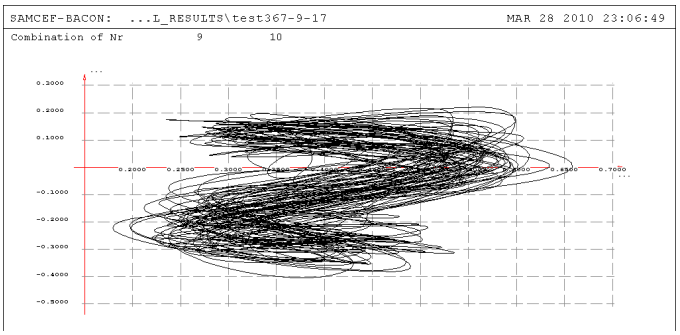

Fig 23 : Subspan 5 - a detailed movement at 17 m/s WIO on the same benchmark case, showing amplitudes peak-to-peak near 0.35 m.

Last but not least, Fig 23 is giving access to a case treated at 17 m/s wind speed showing peak-to-peak amplitudes near 35 cm, roughly in line with observed amplitudes.

5 CONCLUSIONS

Application of quasi-steady theory to the wake-induced oscillations may be re-considered: the new criteria, adopted for aircraft aeroelasticity reveal that, when taking into account the fluid dynamics effects, the quasi-steady approach is questionable, at least at higher frequencies of subspan oscillations.

Model of flutter of leeward cylinder, when directly applied to the finite element model, shows good convergence in the case of a single subspan model. As for extended model of real transmission line span, such model is still subject to improvement. One research direction is aerodynamic loading effects which have to be better integrated into the finite-element model. Second field of research is improvement of the model of line span itself, namely, the spacer model. Perhaps the most important is performing simulations with wake-induced loads adaptation to the different cable models, starting with nonlinear beam element. Current wake force user element, as is realized in Mecano, allows loading any line element (cable or beam).

The series of simulations done with above model of the wake interaction show, that subconductors may easily enter into contact.

An extension of aerodynamic model of the wake to include close-wake has been done, this work is also subject to the future research. As of now, its application to the finite-element model of the line span does not always result in good calculation run due to highly variable forces in the close-wake. A series of adaptations in the numerical data readily available to the numerical simulation is needed.

Future work may also include research to account of non-stationary effects like time delay for a flow to travel between the windward and leeward conductor (flow retardation in the wake).

Finally the complex WIO can be managed by TSO's (Transmission system operators) only by optimisation procedures, based on appropriate spacer location and spacer characteristics. Such procedures can be driven by sensibility matrix builded inside finite element codes.

ACKNOWLEDGMENT

The authors would like to kindly thank the Politecnico di Milano (Pr G. Diana and A. Manenti) as well as the CIGRE AG06 (chair D. Hearnshaw) who provides details about benchmark case to validate the simulations.

REFERENCES

EPRI 2009. Transmission line reference book: Wind-induced conductor motion. Second Edition. EPRI, Palo Alto, CA: 2009. 1018554.

Blevins, R. D. (1990) "Flow-Induced Vibration," Van Nostrand Reinhold, NY

Cigada A.; Diana G.; Falco M.; Fossati F.; Manenti A. (1995) "Vortex Shedding and Wake Induced Vibrations in Single and Bundle Cables," *Proceedings of 9ICWE*, New Delhi, India

Claren, R., Diana, G., Giordana, F., Massa, E. (1971) "The vibrations of transmission line conductor bundles ", *IEEE Trans.-PAS* v. 90, no. 4, 1796-1810

Diana, G., Gasparetto, M. (1972), "Energy method for computing the amplitude of vibration of conductor bundles due to wake effect", *L'Energia Elettrica,* n. 8 - 1972

Diana, G., Bocciolone, M., Cheli, F., Resta, F., Manenti, A. (1999) "The aeroelastic behaviour of the OHTL expanded bundles". *Proc. of the 3rd ISCD (International Symposium on cable dynamics),* Trondheim. pp 97-102

Hardy, C., Boudron, P. (1980) "The Influence of Spacer Dynamic Properties in the Control Of Bundle Conductor Motion", *IEEE Trans. PAS,* v. 99 No.2, p. 790 - 799

Hardy, C., Van Dyke, P. (1995) "Field Observations on Wind-Induced Conductor Motions", *Journal of Fluids and Structures,* v. 9 p. 43-60

Hartlen, R. T., Currie, I. G., "Lift-Oscillator Model of Vortex-Induced Vibration", *ASME Proc. – J. of Eng. Dyn. Div.*, 10, 1970

Hearnshaw, D. (1974) "Spacer dampers performance – a function of in-span positioning", *IEEE Trans. PAS,* v. 93 no.5, 1298-1309

Irvine, H.M. (1988) "Cable Structures", Penerbit ITB Bandung, 1988

Kern, G., et al., (1995) « Nonlinear Flutter in Flow Induced Subspan Oscillations », *Proc. 1st Int. Symp. on Cable Dynamics,* Liege, 1995, 149 – 156

Laneville, A., Brika, D. (2001) «Experimental Simulation of the Fluid and Mechanical Coupling Between Transmission Line Conductors », *Proc. 4th Int. Symp. on Cable Dynamics,* Montreal 2001

Mohajery, M., Rawlins, C. B. (1977) "Transmission Line Having Improved Stability Characteristics From Wake-Induced Subspan Oscillations", US Patent 4 018 980

Newman, D. J., Karniadakis, G. E. (1997) "A direct Numerical Simulation Study of Flow Past a Freely Vibrating Cable*", J. Fluid Mech.* vol. 344, pp. 95 – 136

Price, S.J., (1975) "Wake induced flutter of power transmission conductors", *J. of Sound and Vibration,* 38 (1), 125-147

Price, S.J., Maciel, Y. (1990), "Solution of the nonlinear equations for wake-induced flutter via the Krylov and Bogoliubov method of averaging", *Journal of Fluids and Structures*, 4, pp. 519-540

Price, S.J., Païdoussis, M.P. (1984/1), "An improved mathematical model for the stability of cylinder rows subject to cross-flow", *J. of Sound and Vibration,* 97(4), 615 – 640

Price, S.J., Païdoussis, M.P. (1984/2), "The aerodynamic forces acting on groups of two and three circular cylinders when subject to a cross-flow", *J. of Wind Engineering and Industrial Aerodynamics,* 17, 329-347

Rawlins, C. B. (1976) "Fundamental concepts in the analysis of wake-induced oscillation of bundled conductor", *IEEE Trans. PAS,* v. 95 no.4, 1377-1393

Rawlins, C. B. (1977) "Extended analysis of wake-induced oscillations of bundled conductors", *IEEE Trans. PAS,* v. 96 no.5, 1681-1689

SAMCEF 2009– a general-purpose FEA software, *by SAMTECH S.A.,* rue des Chasseurs-Ardennais, 8, B-4031 Angleur-Liege, Belgium

Simiu, E., Scanlan, R. H. (1996) "Wind Effects on Structures: Fundamentals and Applications to Design", J.Wiley & Sons, NY, 1996

Simpson, A. (1967), "Determination of natural frequencies of multiconductor overhead transmission lines", *Journal of Sound and Vibration*, v. 20(4), 417-449

Simpson, A. (1971/1), "On the Flutter of a Smooth Circular Cylinder in a wake", *Aeronautical Quarterly* XXII, 25-41

Simpson, A. (1971/2), "Wake induced flutter of circular cylinders: mechanical aspects", *Aeronautical Quarterly* XXII, 101-118

Simpson, A., Flower, J.W. (1977), "An improved mathematical model for the aerodynamic forces on tandem cylinders in motion with aeroelastic applications", *J. of Sound and Vibration,* 51(2), 183 – 217

Tsui, Y. T. (1976) Discussion on the article of C. B. Rawlins "Fundamental concepts in the analysis of wake-induced oscillation of bundled conductor", *IEEE Trans. PAS,* v. 95 no.4, 1385-1386

Tsui, Y. T., (1977) "On wake-induced flutter of a circular cylinder in the wake of another", *ASME Trans. – J. Appl. Mech.,* June, 1977, 194 – 200

Tsui, Y. T., (1986) "On wake-induced vibration of a conductor in the wake of another via a 3-D finite element method", *J. Sound and Vibration,* 107(1), 39 – 58

Wardlaw, R. L., Cooper, K. R., Ko, R. G., Watts, J. A. (1975) "Wind Tunnel And Analytical Investigations Into the Aeroelastic Behaviour Of Bundled Conductors", *IEEE Trans. on PAS*, vol. 94 no. 2 p. 642 - 651

Zdravkovich, M. M. (1985), "Flow Induced Oscillations Of Two Interfering Circular Cylinders", *J. of Sound and Vibration,* 101(4), 511-521

Zdravkovich, M. M., (1987), "The effects of interference between circular cylinders in cross flow", J. Fluids and Structures, 1, 239-261

Jean-Louis Lilien (M'1997) , professor, PhD., is the head of the Unit of Transmission and Distribution of Electrical Energy at the Montefiore Institute of Technology, University of Liège, Belgium. He has over 30 years' experience of solving the electrical and mechanical engineering problems of power systems.

His work involves analysis of problems in "cable dynamics" in general and in overhead power lines in particular. His major activities have been devoted to (i) vibrations on transmission lines, in particular galloping, including its control (ii) large movements of cables, such as those forced by short-circuit electromagnetic loading (in both substations and power lines), (iii) health monitoring of power lines (sag and vibrations) and last, but not least, (iv) effects of low-frequency electric and magnetic field on human beings. Jean-Louis is a long-time active member of IEEE and CIGRE, where he has served as convenor of several task forces of CIGRE study committee B2, "overhead lines" and B3 "substations". He has published over 100 technical papers in peer reviewed publications. lilien@montefiore.ulg.ac.be

Dmitry Snegoskiy received his degree in mechanical engineering (physics and continua) from the Moscow Aviation Institute (Russia) in 1994. He is now a PhD student at the University of Liège (Dept. Electricity, Electronics and Computer Sciences, Unit of Transmission and Distribution of Electrical Energy). He participated to IMACS European project (FP6). dvsneg@mail.ru